A Control Strategy for a Distributed Power Generation Microgrid Application With Voltage- and Current-Controlled Source Converter

Emanuel Serban, *Senior Member, IEEE*, and Helmine Serban, *Member, IEEE*

***Abstract*—This paper presents a pseudodroop control structure integrated within a microgrid system through distributed power generation (DPG) modules capable to function in off-grid islanded, genset-connected, and grid-connected modes of operation. System efficiency has an important role in order to harvest the maximum available renewable energy from dc or ac sources while providing power backup capability. A control strategy is proposed in off-grid islanded mode method based on the microgrid line-frequency control as agent of communication for energy control between the DPG modules. A critical case is where the ac load demand could be lower than the available power from the photovoltaic solar array, where the battery bank can be overcharged with unrecoverable damage consequences. The DPG voltage-forming module controls the battery charge algorithm with a frequency-generator function, and the DPG current source module controls its output current through a frequency-detection function. The physical installation between DPG modules is independent, since no additional communication wiring is needed between power modules, which represent another integration advantage within the microgrid-type application.**

***Index Terms*—Distributed power generation (DPG), genset-connected mode, grid-connected mode, hybrid converter, islanded mode, microgrid, photovoltaic (PV) converter, PV inverter.**

I. Introduction

ELECTRICAL power demand within a microgrid power system requires reliable functionality, storage of energy, diagnostics, remote device control, and monitoring as important functions of modern distributed power generation (DPG) modules. Renewable energy sources like solar, wind, and microhydropower can be interfaced through the DPG modules with the microgrid system, which can operate in islanded mode (off-grid) and grid-connected mode. The microgrid operation needs to respond to the load demand under any circumstances; therefore, backup with energy storage elements is essential.

The microgrid presented in this paper is a low-voltage application and it comprises DPG modules, distributed energy storage elements, electrical distribution gear, and controllable loads. DPG modules are critical components within the microgrid systems and need to have flexible features in order to respond for a wide range of applications. DPG are designed to operate in islanded mode, utility grid-connected, or genset-connected (diesel and liquid propane generators) mode.

DPG converter modules may have the following modes of operation: voltage-controlled source, current-controlled source, active rectifier, and active power filter mode. The converted energy produced can be delivered to the local loads within the microgrid structure or exported to the utility grid. In active-rectifier mode with ac to dc energy conversion, the distributed generators has a multiloop-embedded control with power factor correction (PFC), and dc voltage and current are controlled typically for battery charging [1]. In active power filter mode, selective ac current harmonics are generated to cancel out the load current harmonics from the fundamental line frequency [2]. Photovoltaic (PV) inverters are typically DPG, operating in current-controlled mode with dc to ac energy conversion, where ac current is controlled in magnitude and phase [3], [4]. Transformerless PV inverters represent an attractive solution due to higher efficiency, smaller size and weight, and reduced cost [5], [6].

Hybrid converters interface dc energy sources (e.g., PV generators, wind turbines, fuel cells) and ac energy sources (e.g., utility grid, gensets) at both dc and ac ports. In voltage-controlled-source mode, with dc to ac energy conversion, the ac voltage and frequency are controlled to meet the power quality requirements. In this mode of operation, the hybrid converter can operate in islanded microgrid, where multiple modules can be paralleled in order to support the ac loads.

Methods of active current sharing with communication between paralleled modules are available in the technical publications. The advantages of this method are ease of synchronization of paralleled DPG with the grid prior to the transfer, peer-to-peer data interchange between DPGs for centralized microgrid power management, and single-phase to three-phase system conversion with multiple DPG modules [7]. The disadvantage is the need of hardware interconnection between DPGs and droop control methods, which is a more attractive solution in order to avoid the communication signals between multiple paralleled modules [8], [9]. With voltage-controlled source DPG in islanded mode, the ac loads harmonics can be evenly shared among the DPG modules with implementation of enhanced droop harmonic compensation control methods [10].

Manuscript received September 23, 2009; revised December 7, 2009, and April 19, 2010; accepted April 28, 2010. Date of current version December 27, 2010. Recommended for publication by Associate Editor F. Blaabjerg.

E. Serban is with the Schneider Electric's, Renewable Energies Business, Burnaby, BC, Canada (e-mail: Emanuel.Serban@ca.schneider-electric.com).

H. Serban is with the Simon Fraser University, SIAT, Surrey, BC V3T 0A3, Canada (e-mail: hserban@sfu.ca).

Color versions of one or more of the figures in this paper are available online at http://ieeexplore.ieee.org.

Digital Object Identifier 10.1109/TPEL.2010.2050006

0885-8993/$26.00 © 2010 IEEE

Authorized licensed use limited to: N.C. State University Libraries - Acquisitions & Discovery S. Downloaded on June 16,2023 at 18:10:31 UTC from IEEE Xplore. Restrictions apply.

IPR2024-00389
Relink EX2003

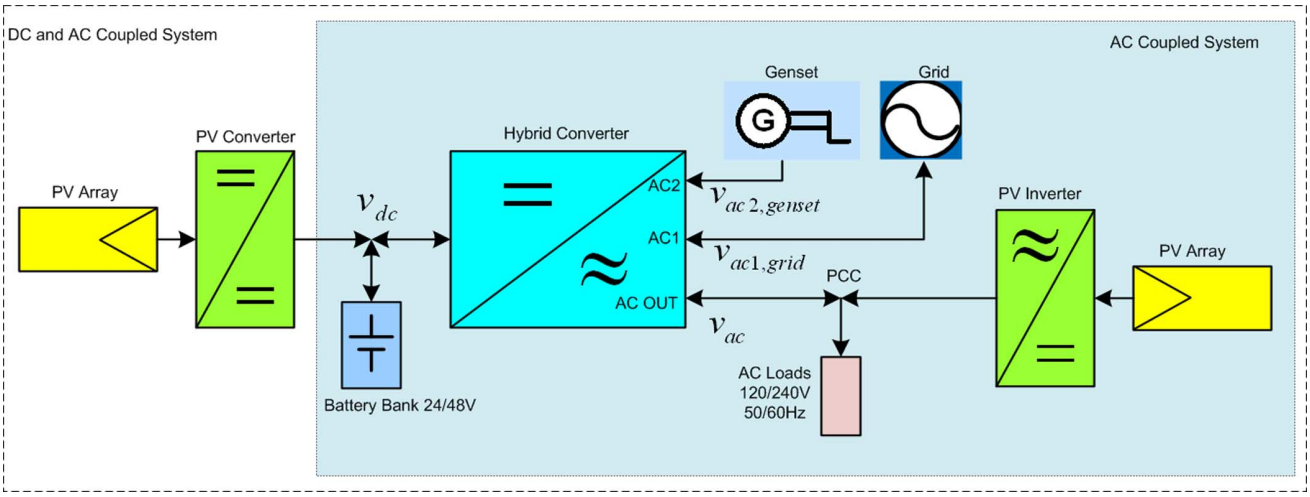

Fig. 1. General block diagram of a microgrid system architecture.

Voltage-controlled source DPGs in grid-connected mode can operate via active and reactive power control [6], [11], [12]. However, some major challenges are related with the droop control methods approach and utility grid requirements. A method of islanding detection is the control of current injection with negative sequence [13], but the effectiveness has not been demonstrated with higher penetration of DPGs or control nuisance due to transient effects within the microgrid structure. The controls of distributed generation systems have to meet the requirements for grid interconnection, for example, UL1741, VDE0126, RD1663, DK5940 Standards for antiislanding, voltage and frequency disconnect, current distortion, dc injection, synchronization, and electromagnetic compatibility immunity on protection functions [14]. At the ac-port connection, the DPGs have to monitor and qualify the available ac source (utility grid or genset) by synchronizing its phase and frequency prior to the transfer event [3], [15].

For higher electrical power demand, multiple DPG can be parallel connected; the ac transfer islanded/grid-connected command among distributed generators units is issued by the system master via controller area network (CAN) bus. For a no-wire communication between the voltage-controlled DPG modules, special attention should be given during the transfer, since the independent voltage-controlled sources do not transfer in the same time.

The goals of this paper are to introduce a new control method based on the microgrid line-frequency variation as the agent of communication for energy control among the DPG modules while presenting the interfacing of solar array using the PV converter and/or PV inverter with hybrid converter system integration. Section II identifies the microgrid elements and DPG modules' functionality, and discusses the microgrid structure for system efficiency maximization. Section III describes the new pseudodroop control proposed structure in comparison to droop control methods. Section IV presents extended feature discussion, the experimental results are presented in Section V, and the conclusions are provided in Section VI.

II. Microgrid System Structure Description

A. Microgrid DPG System Description

The microgrid block diagram illustrated in Fig. 1 is a low-voltage system and comprises DPG modules, distributed energy storage elements (battery bank), and ac loads. DPG modules are pulsewidth-modulated (PWM) converters designed to operate in islanded mode, utility grid-connected, and genset-connected mode.

The hybrid converter is a four-quadrant PWM bidirectional energy converter with integrated ac transfer switches and with the following modes of operation.

1) *Voltage-controlled source converter:* dc to ac energy conversion for inverter-mode islanded backup power application, where the ac voltage and frequency are controlled by the hybrid converter within the microgrid structure (see Fig. 6).
2) *Current-controlled source converter:* dc to ac energy conversion for grid-connected mode, where the ac current is controlled and the ac voltage and frequency are generated by the utility grid or genset. This mode is primarily used when renewable energy is exported from the dc port to the microgrid ac-port network. For example, the PV solar array is connected to the dc battery port via PWM dc/dc PV converter. In Fig. 2, the control structure is partially illustrated, where the ac-current reference $i_{\rm ac}^{*}$ is a function of the dc voltage-loop controller $G_{\rm vd}$ and ac power-loop controller $G_{\rm vp}$, and has integrated antiislanding detection method. The selection function $K_{\rm vp}$ detects the minimum of either output of the dc voltage controller or the ac power controller. The output of the selection function is a normalized value of voltage or power, which is multiplied to the sine-wave generator. For instance, the power loop

Authorized licensed use limited to: N.C. State University Libraries - Acquisitions & Discovery S. Downloaded on June 16,2023 at 18:10:31 UTC from IEEE Xplore. Restrictions apply.

IPR2024-00389
Relink EX2003

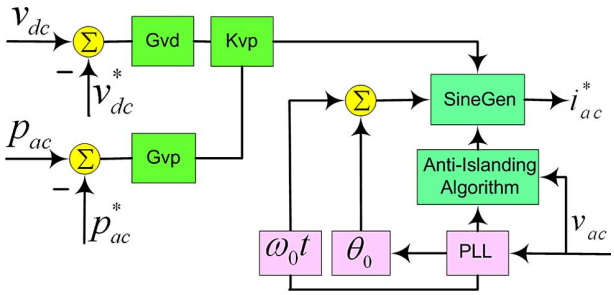

Fig. 2. Current-controlled source inverter mode block diagram of hybrid converter.

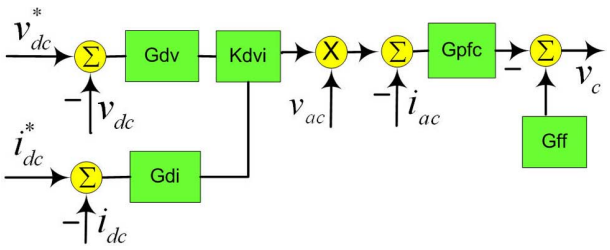

Fig. 3. Active-rectifier mode control block diagram of hybrid converter for battery bank charge.

is required in applications, where the utility grid would not accept dc energy export from a battery port; the reference power $p^*_{\rm ac}$ is set to zero. In this specific case, the dc energy can be transferred only to the ac loads (see Fig. 5).

3) *Active-rectifier mode with PFC:* ac to dc energy conversion, where the dc voltage or current is regulated within the prescribed limits (i.e., battery charge algorithm). In the absence of PV converter, the battery should be recharged from one of the ac ports: in grid-connected mode from utility grid or genset and in islanded mode from the excess of PV inverter energy.

Fig. 3 illustrates a simplified architecture for active-rectifier mode, where the converter has three control loops. The inner PFC control loop ($G_{\rm pfc}$) programs the input ac current to track the ac grid/genset voltage ($v_{\rm ac}$) with near unity power factor. Two low-bandwidth outer control loops are implemented for dc voltage regulation ($G_{\rm dc}$) and dc current regulation ($G_{\rm di}$), for battery bank charge.

In addition, an open-loop feed-forward correction $G_{\rm ff}$ to the control signal v_c is implemented and is proportional to the instantaneous ratio of the input ac voltage and output dc voltage. The selection function $K_{\rm dvi}$ detects the minimum of either output of the dc voltage or current controller for battery charging under constant voltage or current mode.

The PV inverter and PV converter illustrated in Fig. 1 are PWM converters with embedded maximum power point tracking (MPPT) algorithm at the dc input in order to harvest the maximum energy from the PV-array modules. The MPPT algorithm is optimized in order to accommodate fast energy harvesting versus control stability, and sweep the I–V curve to find the global maxima [16], [17].

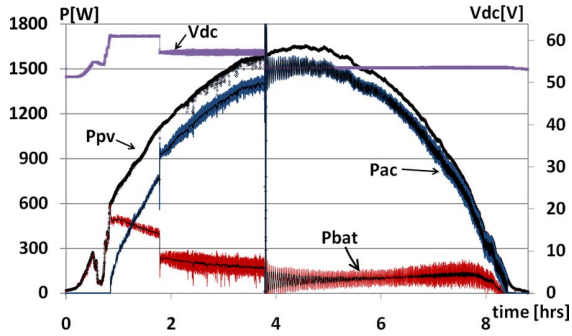

Fig. 4. Daily microgrid operation: power conversion from the solar array. PV converter ($P_{\rm pv}$), battery port ($P_{\rm bat}$), and hybrid converter to ac loads and utility grid ($P_{\rm ac}$).

B. DPG Microgrid System With Solar Array Connected Through the PV Converter to the Energy Storage Element

The microgrid is configured with the PV solar array connected on the dc battery side through a PV converter for power system experimental evaluation.

The PV converter is a dc/dc step-down PWM converter that harvests the energy from the PV-array modules and applies a charging algorithm to the battery bank (e.g., 24 or 48 V). The PV converter regulates the dc battery voltage or current based on the amount of PV power generation or battery state of charge.

When the microgrid is in grid-connected mode, the available energy from the battery bank is transferred to the ac loads or utility grid through the bidirectional hybrid converter, which operates in current-controlled source mode. If the utility grid is in fault condition, then the hybrid converter transfers the microgrid into islanded mode. A seamless transfer of hybrid converter when utility grid fails can be implemented with the indirect current control algorithm [18].

Fig. 4 illustrates a one-day microgrid operation in grid-connected mode with a multicrystalline PV solar array during January in Vancouver, Canada. The PV converter operates in MPPT mode while maintaining the desired multistage charging profile: bulk, absorption, and float. The hybrid converter controls the battery-charging profile while maximizing the harvested energy by forcing the PV converter to constantly remain in MPPT mode. The hybrid converter operates in current-controlled source mode and the amount of the ac current transferred to the ac port is function of the dc battery voltage level for maintaining multistage charging profile (see Fig. 2).

As it can be noticed in Fig. 4, the transferred ac output power follows the input power characteristic of the PV converter. At the beginning of the day, the PV converter charges the battery in bulk (61 V) and absorption phase (57.6 V). When the battery bank is fully charged, the PV converter transitions into float phase (54 V) and the hybrid converter transfers increased power to the ac-bus network, as can be seen in parabolic curve of Fig. 4.

The microgrid structure control architecture achieves increased system efficiency by harvesting the maximum renewable energy while optimally maintaining the battery bank state-of-charge (SoC) and state-of-health (SoH), which is

Authorized licensed use limited to: N.C. State University Libraries - Acquisitions & Discovery S. Downloaded on June 16,2023 at 18:10:31 UTC from IEEE Xplore. Restrictions apply.

IPR2024-00389
Relink EX2003

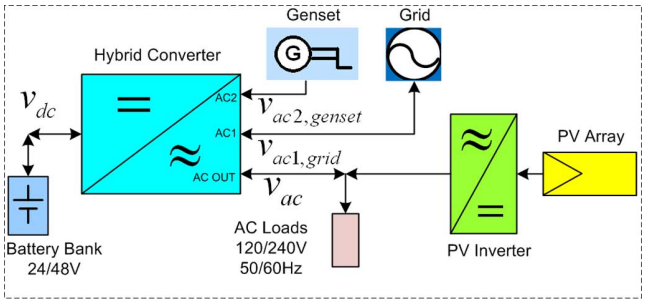

Fig. 5. Block diagram of a microgrid system with hybrid converter and PV inverter.

represented by

$$\mathrm{SoC}(t) = \mathrm{SoC}(t_0) - \frac{1}{Q_N}\int_{t_0}^{t} i_{\mathrm{bat}(t)}dt$$

$$\mathrm{SoH}(t) = \frac{Q(t)}{Q_N} \tag{1}$$

where Q_N is the nominal ampere-hour fully charged battery capacity. $i_{\mathrm{bat}(t)}$ is the discharge battery current, $\mathrm{SoC}(t_0)$ is the nominal capacity at initial time t_0.

The advantage of this microgrid structure is excellent preservation of battery bank SoC and SoH for reliable backup power transfer to the ac critical loads. The disadvantage of this architecture is system efficiency loss due to battery-charging/discharging losses and DPG lower efficiency, since the ratio of the power conversion varies within a wide range.

The system average efficiency from the PV-array generator to the ac bus is around 92% while the battery is in float mode, and it can be observed that there is about 100 W power losses due to battery bank idle charge.

An alternative to the microgrid system configuration is presented in Fig. 5 for system efficiency improvement, with the solar energy being transferred to the ac-bus network by a PV inverter.

C. DPG Microgrid System With Solar Array Connected Through the PV Inverter

The microgrid is configured with the solar array connected at point of common coupling (PCC) ac bus through PV inverter for maximizing the system conversion efficiency.

When the utility grid is present, the hybrid converter qualifies the ac grid and transfers the microgrid into grid-connected mode. The ac loads can be powered by both PV inverter and utility grid. The hybrid converter is in active-rectifier mode by charging the battery bank with the maximum of the difference between ac breaker size current I_{BR} and load demand current $I_{\text{ac-loads}}$ in order not to exceed the allowable grid current. The dc battery charge reference $I^*_{\mathrm{dc,ref}}$ can be a derated function of the ac current I_{ac}, ac voltage V_{ac}, and the temperature of internal components T_i

$$I_{\mathrm{ac}} = I_{\mathrm{BR}} - I_{\text{ac-loads}}$$

$$I^*_{\mathrm{dc,ref}} = F(I_{\mathrm{ac}}, V_{\mathrm{ac}}, T_i). \tag{2}$$

If the utility grid fails, the microgrid is transferred into islanded mode and the hybrid converter operates in voltage-controlled mode. If the ac load demand exceeds the available energy from PV and battery bank, then the genset is automatically started.

In genset-connected mode, the PV inverter can backfeed the genset, which is undesirable. The hybrid converter has integrated transfer switches on both ac ports, AC1 and AC2, which can prevent this scenario by disconnecting genset AC2 port, since the ac current is continually monitored to all ports: AC1, AC2, and AC Out (see Figs. 1 and 5). If the load demand exceeds the power capability of the genset and PV inverter, then the hybrid converter turns into genset support mode as a current-controlled source by converting the energy from dc to ac port. In this mode of operation, the power loop (see Fig. 2) adjusts the ac current reference by the selectable reference power P^*_{ac} in order to avoid genset ac overload. The hybrid converter power loop is tuned in order to achieve the stable dynamics under load demand and genset backfeed rejection under load disconnect.

If the utility grid and genset ac sources are not present, then the sources of energy for the ac loads consist of the solar array and battery bank.

The availability of energy is always limited and intelligent systems have to be designed to optimally process it, but there are cases where the extra energy presence within microgrid systems may damage the electrical devices.

In islanded mode, there is an issue when active power, referred at the PCC, from the PV-array (p_{pv}) cannot be consumed or stored by the ac loads ($p_{\text{ac-loads}}$), dc loads ($p_{\text{dc-loads}}$), and battery bank (p_{storage})

$$p_{\text{PV-Inv}}(t) > p_{\text{ac-loads}}(t) + p_{\text{dc-loads}}(t) + p_{\mathrm{storage}}(t). \tag{3}$$

A solution is to have wired communication between these electrical systems to prevent and limit the excessive energy [19]; another solution is to dump the energy surplus into resistive loads. A more attractive solution is proposed to use the microgrid line frequency as an agent of communication for the control of variables with no wire communication between DPGs.

III. DPG Control Methods and Control Structure Implementation

In islanded mode, the hybrid converter operates in voltage-controlled source mode by controlling the ac voltage and frequency. The PV inverter harvests the dc solar energy and operates in ac current-controlled mode. The ac loads have a dynamic operation: energy can be sourced by one or both of the sources, i.e., solar array and battery bank.

If the solar energy is greater than the load demand, then the surplus of power will flow from PCC through the bidirectional hybrid converter charging the battery bank (3). In this case, the battery bank can be overcharged, which causes gassing, water loss, plate grid corrosion, all of which shorten its lifetime.

A control method in microgrid applications is achieved by voltage-controlled source converters operating in droop mode by controlling the active power direction based on the battery voltage regulation. When the battery voltage increases over a

Authorized licensed use limited to: N.C. State University Libraries - Acquisitions & Discovery S. Downloaded on June 16,2023 at 18:10:31 UTC from IEEE Xplore. Restrictions apply.

IPR2024-00389
Relink EX2003

specified value, due to surplus of energy at PCC, the line frequency is changed and is a function of the active/reactive powers flow within the hybrid converter [20]. This method has to be improved, since the line frequency has variations (e.g., ± 1 Hz) greater than the antiislanding limits and the magnitude of ac-bus voltage has variations as well (e.g., $\pm 6\%$ $V_{\rm PCC}$).

For a voltage-controlled source, connected at a common ac bus, the complex power flowing into the power line at PCC can be expressed by the relation

$$\underline{S}_{\rm PCC} = \frac{V_{\rm conv}V_{\rm PCC}}{Z}e^{j\theta} - \frac{V_{\rm PCC}^2}{Z}e^{j(\theta-\phi)} \tag{4}$$

where $V_{\rm conv}$ and $V_{\rm PCC}$ represent the amplitude converter output voltage and at the PCC, respectively, $\phi = \measuredangle(\bar{V}_{\rm conv}, \bar{V}_{\rm PCC})$ is the power angle, Z and θ represent the magnitude and phase of the converter output impedance. The active and reactive powers are deduced from (4) and represented as follows:

$$P_{\rm conv} = \frac{V_{\rm conv}V_{\rm PCC}}{Z}\cos(\theta-\phi) - \frac{V_{\rm PCC}^2}{Z}\cos\theta$$
$$Q_{\rm conv} = \frac{V_{\rm conv}V_{\rm PCC}}{Z}\sin(\theta-\phi) - \frac{V_{\rm PCC}^2}{Z}\sin\theta. \tag{5}$$

The relationship between voltage, frequency, and active and reactive power can be viewed through the following two cases.

1) In the conventional droop methods, the converter output impedance is considered to be inductive with the reactance X, $Z = jX$

$$P_{\rm conv} = \frac{V_{\rm conv}V_{\rm PCC}}{X}\sin\phi$$
$$Q_{\rm conv} = \frac{V_{\rm PCC}(V_{\rm conv}\cos\phi - V_{\rm PCC})}{X}. \tag{6}$$

Equation (7) shows the dependency between active power and the line frequency and is not a straightforward approach to achieve all the following conditions: dc voltage/current regulation, current sharing, tight ac voltage/current regulation, and maximum active power transmission from the PV panels to the storage element.

$$\omega = \omega_0 - mP_{\rm conv}$$
$$V_{\rm conv} = V_{0\rm conv} - nQ_{\rm conv} \tag{7}$$

where ω_0 represents the no-load angular frequency, $V_{0\rm conv}$ is the converter output voltage at no load, m is the frequency droop coefficient, and n is the voltage droop coefficient. Power control strategies have been implemented with a virtual inductance to prevent P–Q coupling and voltage-drop compensation due to the active power flow in resistive low-voltage microgrids [21].

2) If the output impedance of the converter is considered/programmed resistive, $Z = R$ with $\theta = 0$ and small power angle, then the active power is decoupled from the line frequency

$$P_{\rm conv} = \frac{V_{\rm PCC}(V_{\rm conv}\cos\phi - V_{\rm PCC})}{R}$$
$$\approx \frac{V_{\rm PCC}(V_{\rm conv} - V_{\rm PCC})}{R}$$
$$Q_{\rm conv} = -\frac{V_{\rm conv}V_{\rm PCC}}{R}\sin\phi \approx -\frac{V_{\rm conv}V_{\rm PCC}}{R}\phi. \tag{8}$$

Therefore, when the converter output impedance is highly resistive, the P–Q droops exchange their characteristics [22], [23]

$$\omega = \omega_0 + mQ_{\rm conv}$$
$$V_{\rm conv} = V_{0\rm conv} - nP_{\rm conv}. \tag{9}$$

In this case, the output impedance of the voltage source converters is programmed through the control loops: resistive impedance for active power sharing (P–V) and inductive impedance for reactive power sharing (Q–ω).

As can be seen from the relations (6)–(9), the droop control methods are line-frequency dependent in order to achieve load sharing while no communication is required between the voltage source converters. However, in distributed power systems applications, the microgrid might be required to operate in both islanded and grid-connected mode. In practice, low-bandwidth communication between the voltage source converters is implemented, e.g., for system data management and grid synchronization [24].

The proposed control method is a pseudodroop control having the appearance of the droop control methods, since the line frequency is primarily used as a communication control agent for energy flow regulation.

Droop control methods can be implemented as well, but more attention has to be paid to the control implementation, where the line frequency is primarily used for P–Q sharing-transmission control, and then it could be used for the dc voltage/current regulation.

In islanded mode, some of the proposed control method features are as follows.

1) Frequency pattern can have linear or nonlinear signature for a more redundant control. For instance, in genset-connected mode the nonlinear pattern is recommended, since the line frequency is much less regulated than other ac sources (due to load changes, genset droop controls), where the PV inverter might misinterpret the linear frequency variation (e.g., unnecessary transitioning from MPPT to power limit mode and reducing its output power and not harvesting the maximum available solar energy.
2) Independent control of the line frequency with respect to the active power flow in both cases, i.e., stand-alone or paralleled hybrid converters operation with very good microgrid line frequency and voltage regulation. In case of parallel operation, the active current sharing between the hybrid converters is achieved by CAN communication. The communication also facilitates the synchronization transfer of the islanded microgrid to the grid-connected mode [7].
3) Power flow control operation within the antiislanding limits: dc voltage and current regulation with programmable values, e.g., multistage battery charging.

In general, both line frequency and voltage variation can be used as interaction parameters between the hybrid converter and PV inverter (12). For instance, in islanded mode, when the PV

Authorized licensed use limited to: N.C. State University Libraries - Acquisitions & Discovery S. Downloaded on June 16,2023 at 18:10:31 UTC from IEEE Xplore. Restrictions apply.

IPR2024-00389
Relink EX2003

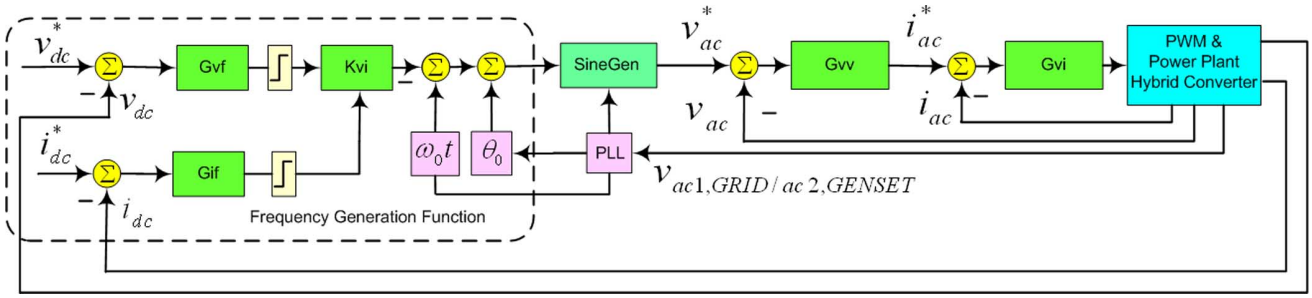

Fig. 6. Hybrid converter with FGF control structure in voltage-controlled islanded mode.

inverter produces greater energy than the load demand, the active power flows to the battery and the dc voltage or current can exceed the system requirements (3). The hybrid converter proactively monitors and applies the correct charging profile: if the dc voltage or current exceed the limit charging battery requirements, then the hybrid converter would change the microgrid line frequency (4). The PV inverter may disconnect, since the line frequency would exceed its frequency range limits or it may reduce its current produced from the solar array if a specific control is implemented by monitoring the line frequency, the agent of communication control. It can be noted that the voltage magnitude variation can be used as an agent of communication instead between the DPG modules. However, this method is less accurate than sensing the frequency due to the voltage drop being a function of the power wiring characteristics.

A. Implementation of Frequency-Generation Function Control Structure in the Hybrid Converter

A line-frequency control variation method is proposed as an agent of communication between the hybrid converter and the PV inverter. This method requires no additional wiring for communication, and the DPG modules can be placed far away from each other: the hybrid converter with the battery bank at one location and the PV inverter with the solar array at a different location.

In islanded mode, the hybrid converter has the control over ac microgrid line frequency and voltage regulation. When the PV inverter produces greater energy than the load demand, the active power flows to the battery bank: the hybrid converter operates in two modes at the same time: inverter mode ac voltage/frequency regulation and active-rectifier mode charging the battery.

A frequency-generation function (FGF) is proposed as a control structure within the hybrid converter, which becomes active only when the following two conditions are satisfied (10)

1) Active power flows from the ac port to dc port (by convention $P_{\rm conv} > 0$).
2) Dc voltage (e.g., absorption, float) or dc-current-charge level exceeds a certain set point limit

$$\begin{aligned} &\text{if} \quad P_{\rm conv} > 0 \\ &\quad v_{\rm dc}(t) > V^*_{\rm dc} \text{ or } i_{\rm dc}(t) > I^*_{\rm dc}, \\ &\text{then} \quad \text{FGF} = \text{enabled}. \end{aligned} \tag{10}$$

The FGF controls the microgrid line frequency by decreasing or increasing its nominal value $f_0 = 50/60$ Hz. The FGF can have a linear or nonlinear response. Fig. 6 illustrates the implementation of the control for the hybrid converter, which operates in voltage-controlled source inverter mode. The PCC ac network voltage $v_{\rm ac}$ is compared with the reference and the error is compensated by the voltage controller $G_{\rm vv}$ whose output becomes the ac current reference $I^*_{\rm ac}$; the difference between $I^*_{\rm ac}$ and inductor ac current $i_{\rm ac}$ is compensated by the current controller $G_{\rm vi}$, which generates the duty cycle command. The hybrid converter output voltage $v_{\rm ac}$ in voltage-controlled inverter source mode is represented by two terms: the first term multiplied with the ac sine-wave voltage reference $v^*_{\rm ac}$ is desired to be close to unity for output voltage reference tracking, while the second term multiplied with the ac output current i_0 is desired to be close to zero for load disturbance decoupling

$$\begin{aligned} v_{\rm ac}(s) = &\frac{G_{\rm vv}(s)G_{\rm vi}(s)}{s^2{\rm LC} + s\cdot C\cdot G_{\rm vi}(s) + G_{\rm vv}(s)G_{\rm vi}(s)} v^*_{\rm ac}(s) \\ &- \frac{sL + G_i(s)}{s^2{\rm LC} + s\cdot C\cdot G_{\rm vi}(s) + G_{\rm vv}(s)G_{\rm vi}(s)} i_0(s) \end{aligned} \tag{11}$$

where LC represents the output filter and Laplace operator s is approximated with $j\omega$, angular frequency ω. The sine-wave voltage tracking and dynamic load disturbances decoupling control implementation has to be robust and stable, since the PV inverter antiislanding method actively tends to destabilize the voltage and frequency regulation in islanded operation mode.

The generic expression for the sinusoidal ac output voltage generated by the voltage source converter could contain both frequency and amplitude modulation

$$v_{\rm ac}(t) = (V + \hat{v}(t))\sin[(\phi(t) + \theta_0(t)]. \tag{12}$$

The ac output voltage is desired to be constant at steady-state value V with negligible voltage perturbation $\hat{v}(t)$ with the phase variable defined as the integral of the instantaneous angular line frequency $\omega_0(t)$

$$\begin{aligned} \phi(t) &= \int \omega_0(t)dt \\ \omega_0(t) &= 2\pi f_0(t) = \frac{d\phi(t)}{dt}. \end{aligned} \tag{13}$$

The phase angle $\theta_0(t)$ is a time variable when the hybrid converter synchronizes its voltage with the utility grid prior to the transfer from islanded mode to grid-connected mode.

Authorized licensed use limited to: N.C. State University Libraries - Acquisitions & Discovery S. Downloaded on June 16,2023 at 18:10:31 UTC from IEEE Xplore. Restrictions apply.

IPR2024-00389
Relink EX2003

If the sense of the real power flow changes, i.e., the hybrid converter sinks current and dc battery voltage/current reaches $V^*_{\rm dc}/I^*_{\rm dc}$ maximum prescribed values, then the output of FGF $K_{\rm vi}$ linearly decrease the reference frequency f_0. A proportional-integral (PI) controller is digitally implemented for both dc voltage and current controller with, respectively, proportional k_P and integral k_I gains and selector function $K_{\rm vi}$. The sine-wave reference $v^*_{\rm ac}(t)$ is generated by a lookup table with the modulating index m_i, amplitude scale reference V_M, and phase angle θ_0

$$v^*_{\rm ac}(t) = mV_M \sin[2\pi(f_0 - |K_{\rm vi}(t)|)t + \theta_0]. \tag{14}$$

In this example, the frequency $f_0(t)$ would decrease from its nominal value if the monitored dc voltage and current exceeds the maximum prescribed values $(V^*_{\rm dc}/I^*_{\rm dc})$; conversely, the control can accommodate an increase of frequency if desired. The selector function $K_{\rm vi}$ is given by

$$K_{\rm vi}(t) = \min\{K_v(t), K_i(t)\}. \tag{16}$$

The output of the dc voltage and current controller clamped is represented by the relations (16) and (17)

$$K_v(t) = \begin{cases} x_v(t), & x_v(t) < 0 \\ 0, & x_v(t) \geq 0 \end{cases} \tag{16}$$

$$K_i(t) = \begin{cases} x_i(t), & x_i(t) < 0 \\ 0, & x_i(t) \geq 0. \end{cases} \tag{17}$$

The output of the dc voltage or current controller is represented by the relation (18)

$$x_v(t) = k_{Pv}e_v(t) + \int k_{Iv}e_v(t)dt$$

$$x_i(t) = k_{Pi}e_i(t) + \int k_{Ii}e_i(t)dt. \tag{18}$$

The dc voltage reference $V^*_{\rm dc,ref}$ represents the bulk, absorption, float, equalize, or any desired voltage level, which can be accordingly adjusted based on the battery type. The reference values are also temperature-compensated with the coefficients k^T_v, k^T_i determined by the battery chemistry in order to achieve an optimized charge profile (e.g., $k^T_v = -0.108$ V/°C for 48 V lead-acid-flooded battery).

$$V^*_{\rm dc} = V^*_{\rm dc,ref} + \Delta T k^T_v$$

$$I^*_{\rm dc} = I^*_{\rm dc,ref} + \Delta T \cdot k^T_i \tag{19}$$

$$\Delta T = T_{\rm bat} - T_{25C}$$

$$(k^T_v, k^T_i) < 0 \tag{20}$$

The dc current reference $I^*_{\rm dc}$ represents the maximum current limit acceptable to the battery bank.

The difference between the reference and the instantaneous value represents the error value applied to the PI compensator

$$e_v(t) = V^*_{\rm dc} - v_{\rm dc}(t)$$

$$e_i(t) = I^*_{\rm dc} - i_{\rm dc}(t). \tag{21}$$

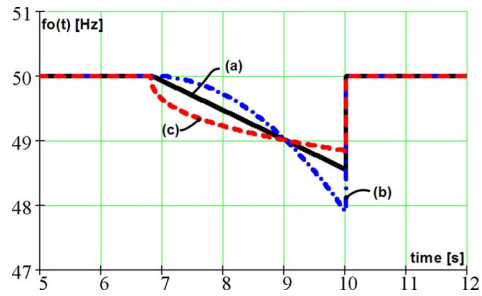

Fig. 7. Frequency-time generation pattern. (a) Linear $\alpha = 1$. (b) and (c) Exponential $\alpha = 2$, $\alpha = 0.4$.

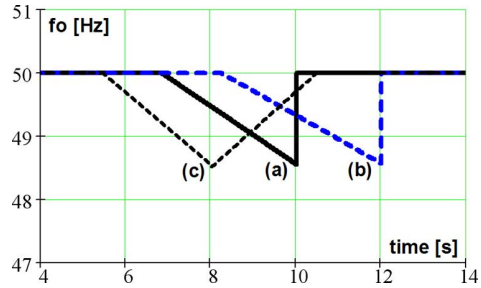

Fig. 8. Frequency-generation linear-type function dependance of dc charge voltage/current $d(v_{\rm dc}, i_{\rm dc})/dt$ rate: (a) $dv_{\rm dc}/dt = 0.3$ V/s, (b) $dv_{\rm dc}/dt = 0.25$ V/s (c) $dv_{\rm dc}/dt = 0.375$ V/s with symmetrical frequency recovery.

Fig. 7 illustrates the frequency function response with a linear ($\alpha = 1$) or exponential response ($\alpha > 1$)

$$f_0(t) = f_0 - [K_v(t)]^\alpha$$

$$f_0(t) = f_0 - [K_i(t)]^\beta. \tag{22}$$

Fig. 8 illustrates the rate of change of frequency response as function of the dc voltage variation. If the voltage/current error is large, then the microgrid line frequency $f_0(t)$ is controlled rapidly. In this example, the frequency is linearly decreased and the rate of change can be a combination between linear exponential response by having the coefficients α and β function of the instantaneous dc voltage and current. The frequency response can be implemented with symmetrical recovery as can be noted in Fig. 8 (Note that dc voltage regulation would require a control of input power, but this solution is not acceptable, since it would not regulate the ac-bus voltage necessary for critical loads).

B. Implementation of Frequency-Detection Function Control Structure in the PV Inverter

Grid-connected DPG modules that convert power to the utility grid are required to have implemented means of islanding detection. The line-frequency range, where DPG modules are allowed to transfer power is limited and have different requirements: the minimum and maximum frequency range for 50-Hz grid systems can be 51–48 Hz or for 60-Hz grid systems can be 60.5–59.3 Hz [14]. The frequency range below its nominal value is larger; therefore, the PV inverters have wider operation range below 50/60 Hz.

Authorized licensed use limited to: N.C. State University Libraries - Acquisitions & Discovery S. Downloaded on June 16,2023 at 18:10:31 UTC from IEEE Xplore. Restrictions apply.

IPR2024-00389
Relink EX2003

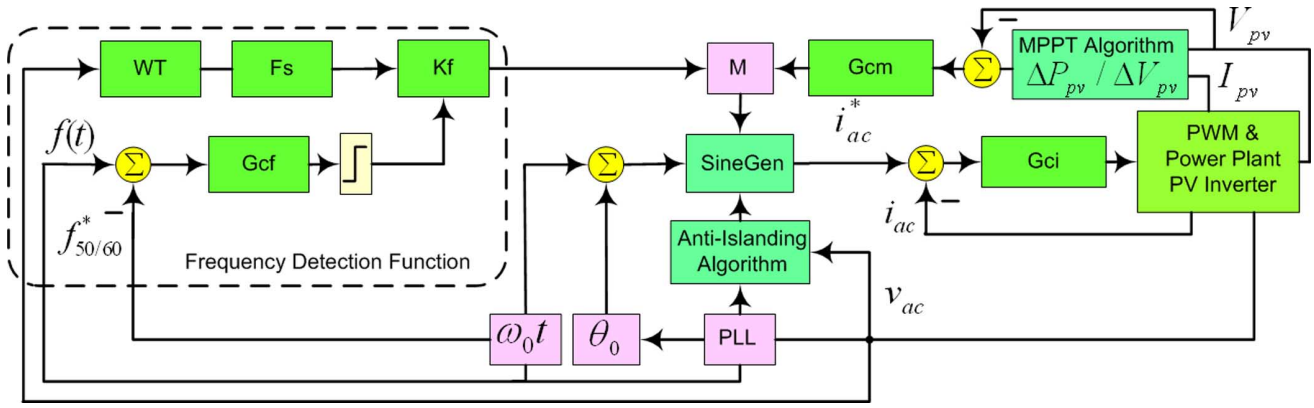

Fig. 9. PV inverter with frequency-detection function control block diagram.

In islanded mode, the microgrid line frequency is set by the hybrid converter; only when the dc voltage or current is exceeded, the frequency starts to decrease linearly. When the minimum frequency limit is reached, the PV inverters disconnect from the ac network ceasing the power to the dc port, and the frequency is restored back to the nominal value. It can be noted that the hybrid converter varies its frequency in the wider range of allowable PV operational range, e.g., 50–48 Hz. The hybrid converter transfers the surplus of energy from ac network to dc port and charge occurs up to the absorption phase while the battery is about 80% charged, since it finishes the bulk-charging phase.

A complete charge profile would require the regulation of the dc voltage for absorption and float-charging phases. In this scenario, PV inverters have to access the dc voltage information for controlling its local ac current. Communication is required to perform the battery voltage regulation and wireless protocols or wire connection can be implemented. These methods are not considered in this paper, since a more redundant mode of operation is proposed: the agent of communication is the line-frequency variation within the range of antiislanding limits. The microgrid voltage pattern variation can be used as an agent of communication, but is less precise than the frequency, since it is subjected to the wire impedance variation due to the load demand. A frequency-detection function is proposed for implementation in the PV inverter, which will sense a specific frequency change pattern and to adjust its local ac current, exiting from the MPPT mode to ac-coupling mode. Under ac-coupling mode, the hybrid converter would alternate the frequency change slope over a determined integrated period in order to average the microgrid line frequency to its nominal value 50/60 Hz.

Fig. 9 illustrates the control implementation for the PV inverter that operates as current-controlled source. The sine-wave current reference $I^*_{\rm ac}$ generated by the SineGen lookup table is synchronized with the grid frequency $f(t)$ and phase θ_0 to achieve unity power factor. A specific frequency pattern is generated by the hybrid converter and should be accurately sensed by the frequency-detection function, since the PV inverter will exit from MPPT mode and will regulate its local output function of the frequency pattern variation. If the frequency variation does not follow a specific pattern, the selection function M selects the MPPT mode for controlling the ac output current.

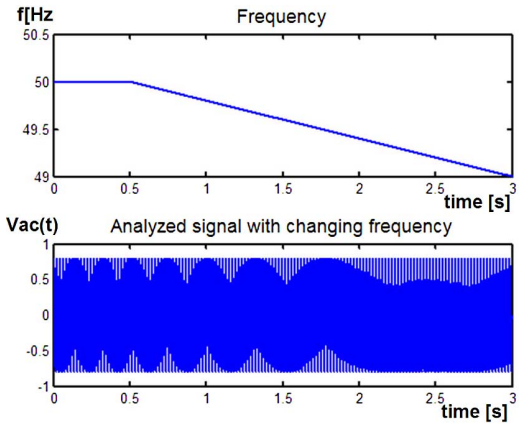

Fig. 10. Frequency change characteristic and sampled microgrid ac voltage.

Among the control alternatives, PID type control, fuzzy logic, FFT, etc., a wavelet method for frequency change detection can be implemented.

Wavelets transforms have excellent frequency-time localization and tracking for rapid changing signals [19].

The line-frequency change detection can be realized with PI frequency controller $G_{\rm cf}$ or more accurately with a wavelet frequency tracking *WT* and pattern-selection function F_S.

When the specific line-frequency pattern is detected, the frequency coefficient K_f controls the output current of the PV inverter.

A continuous wavelet transform is applied to the sensed signal from (11). As a result of this process, the wavelet coefficients $C(a,b)$ are generated, where parameter a is the scale and b the position.

$$C(a,b) = \int_{-\infty}^{\infty} v_{\rm ac}(t)\psi^*_{ab}(t)dt \tag{23}$$

where $\psi^*_{ab}(t)$ is the complex conjugate of wavelet function $\Psi_{ab}(t)$, which is used as the analysis tool and should detect the frequency change in any time interval (see Fig. 10).

Authorized licensed use limited to: N.C. State University Libraries - Acquisitions & Discovery S. Downloaded on June 16,2023 at 18:10:31 UTC from IEEE Xplore. Restrictions apply.

IPR2024-00389
Relink EX2003

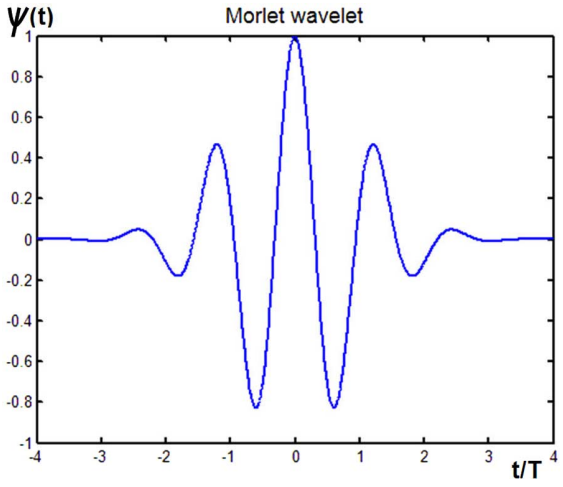

Fig. 11. Morlet wavelet.

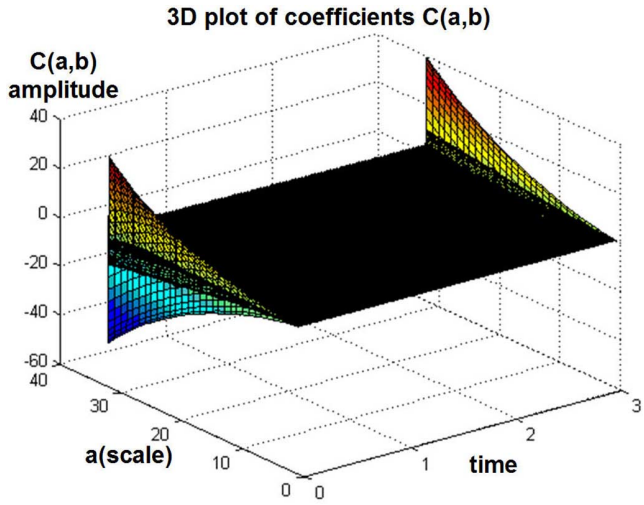

Fig. 12. Surface plot of wavelet coefficients $C(a, b)$.

The original wavelet function is $\Psi(t)$ with the scale parameter $a = 1$ and position $b = 0$.

The weighting factor $1/\sqrt{a}$ of wavelet function $\Psi_{ab}(t)$ ensures that the wavelets have the same energy at every scale

$$\psi_{ab}(t) = \frac{1}{\sqrt{a}}\psi\left(\frac{t-b}{a}\right). \tag{24}$$

The oscillation of the wavelet gives the frequency content of $v_{\rm ac}(t)$, and the values of the wavelet coefficients will reflect how closely correlated the wavelet is with a particular section of the signal, as given by the position parameter.

The proposed frequency detection method makes use of the Morlet wavelet transform [25], [26]

$$C(a,b) = \frac{1}{\sqrt{a}}\int_{-\infty}^{\infty} v_{\rm ac}(t)e^{-[(t-b)/a]^2/2}e^{j\omega[(t-b)/a]}dt. \tag{25}$$

Equation (25) measures the similarities between the basis wavelet function and sensed signal $v_{\rm ac}(t)$. The Morlet wavelet basis function is given (26), where f_0 is the central frequency of the wavelet (e.g., the nominal line frequency $f_0 = 50$ Hz) and f_b is a bandwidth parameter, e.g., 49–50 Hz)

$$\psi(t) = \frac{1}{\sqrt{\pi f_b}}e^{2\pi f_0 t}e^{\frac{-t^2}{f_b}}. \tag{26}$$

Fig. 11 shows the finite duration of the wavelet. The Fourier transform of the Morlet wavelet is given by (27), which reflects the characteristics of a bandpass filter with central frequency f_b

$$\psi(f) = e^{-\pi^2 f_b (f-f_0)^2}. \tag{27}$$

The algorithm for frequency-change detection using the Morlet wavelet transform is described in the following section. The Morlet wavelet transform is applied to the signal $v_{\rm ac}(t)$. The wavelet coefficients are illustrated as a surface plot in Fig. 12, in the time-scales space: output of the Morlet wavelet transform are represented by the coefficients $C(a,b)$.

In this case of application, the purpose is to track fine frequency changes, and low values of parameter a will have the effect of compressing the wavelet for small frequency-change detection.

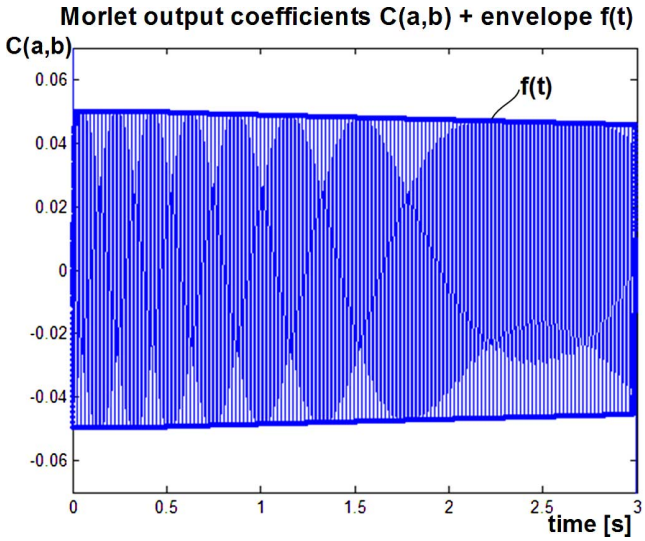

Fig. 13. Time domain plot of wavelet coefficients $C(a, b)$, $a = 1$, where the envelope reflects the linear change of the frequency pattern.

Therefore, coefficients corresponding to the scale parameter a of level 1 ($a = 1$) are of interest in this case.

For the position parameter b, 100 samples per line cycle is selected. The local maxima and minima of these coefficients are computed and represented in Fig. 13. A polynomial best-fit function of the envelope $f(t)$ is searched for and this function will reflect the variation in time of the original signal frequency [27]. For example, if the frequency has a linear pattern of change, a mathematical expression of the linear type can be constructed.

IV. Discussion

The overall control stability has to be viewed with the following considerations: individual DPG stability and the system stability in islanded mode interaction.

Authorized licensed use limited to: N.C. State University Libraries - Acquisitions & Discovery S. Downloaded on June 16,2023 at 18:10:31 UTC from IEEE Xplore. Restrictions apply.

IPR2024-00389
Relink EX2003

The proposed method has negligible impact on the individual DPG stability, since the line-frequency (50/60 Hz) change has a relatively slow, e.g., $\Delta f_0/\Delta t < 1$ Hz/s and small frequency variation ($<2\% f_0$) with respect to the bandwidth response of DPG control loops. Therefore, the frequency-step perturbation has negligible impact to the individual control stability DPG system components and tolerable frequency change to transformers or other ac loads. The microgrid line-frequency variation of the presented method with up to 2% can be further compensated by a digital moving average function to keep the average frequency at its nominal value.

The system stability in islanded mode interaction and the active power transferred from the PV inverter to the battery through the hybrid converter may occasionally fluctuate and this can be perceived as system instability. The power oscillation could be caused by the battery impedance, ac load dynamics, FGF rate of change, and the frequency-detection function response.

In order to eliminate the power oscillation effect, with digital control implementation, the proportional (e.g., k_{Pv}, k_{Pi}) and integral (e.g., k_{Iv}, k_{Ii}) control gains from (12) are adaptively changed. These gains are adaptively updated and they are function of: the battery impedance (or battery capacity) and the real power, which is transferred to the battery.

When the battery impedance is higher (due to aging factor or lower battery capacity), the dc voltage rate of change (dV_{dc}/dt) is higher; similarly, the ac power rate of change (dP_{ac}/dt) depends of the ac loads activity and PV Inverter MPPT algorithm. It should be noted that the microgrid is less damped when ac loads diminishes. The selection of proportional and integral gains is selected as a tradeoff between the stability margin and good dynamic performance: low gains with increased response time and poor transient behavior versus high gains with less margin stability.

The battery impedance can be periodically estimated through analysis of dc current and voltage measurements while the battery is cycled and the control gains are updated.

The control method presented can be implemented for single-phase and three-phase systems without additional hardware or communication wiring between hybrid converter and PV inverter with built-in control function for higher reliability power systems operation.

V. Experimental Results

The control and architecture for both hybrid converter and PV inverter was implemented and tested on bidirectional 6-kVA Schneider Electric Xantrex XW6048-230-50 converter module, ac port configured at 230 V/50 Hz and dc port 40–65 V connected to a 225-Ah lead acid battery bank. The control firmware implemented is using a 32-bit TMS320F2812 DSP running at 150 MHz.

Stable and good dynamic transitions of the power flow are achieved between the DPG modules: Fig. 14 is illustrates the scenario when ac load suddenly disconnects and the battery voltage rises up to the maximum dc set point corresponding to the bulk, absorption, or float voltage level. The hybrid converter varies the microgrid frequency outside the limits of the acceptable operation limits set in the PV inverter, and the transfer power from ac to dc port is ceased.

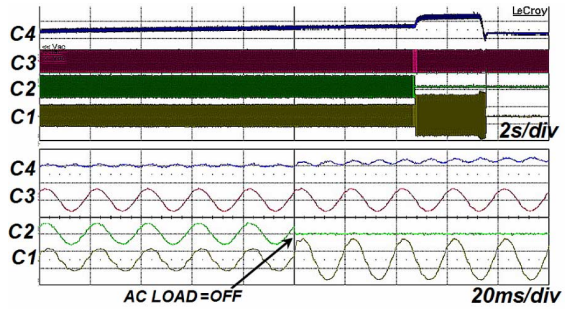

Y-axis: C1: Iac 10A/div C2: I_{LOAD} 10A/div
C3: Vac 500V/div C4: Vdc 5V/div

Fig. 14. Experimental results in off-grid islanded mode: ac step-load response. y-axis: C1—I_{ac} 10 A/div, C2—I_{LOAD} 10 A/div, C3—V_{ac} 500 V/div, and C4—V_{dc} 5 V/div.

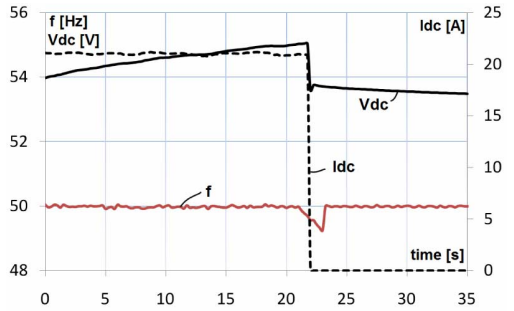

Y-axis: f: 1Hz/div Vdc: 1V/div, Idc: 5A/div

Fig. 15. Experimental results in off-grid islanded mode: dc-voltage line-frequency response, no ac load connected. y-axis: f—1 Hz/div, V_{dc}—1 V/div, and I_{dc}—5 A/div.

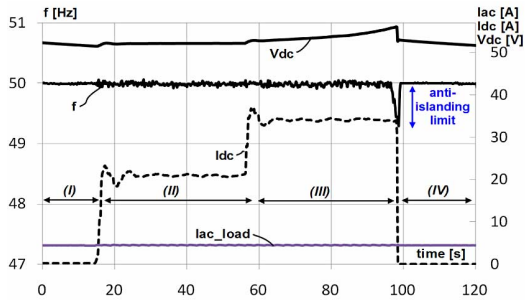

Y-axis: f: 1Hz/div Vdc: 10V/div, Idc: 10A/div, Iac: 10A/div

Fig. 16. Experimental results in off grid islanded mode: dc-voltage line-frequency response, with ac load connected. y-axis: f—1 Hz/div, V_{dc}—10 V/div, and I_{dc}—10 A/div, and I_{ac}—10 A/div.

The experimental results show a stable system behavior under different dynamic conditions: Figs. 15 and 16 show the effect of the FGF, where the hybrid converter linearly changes the microgid frequency with a rate of change equal with 0.4 Hz/s.

The phase transitions illustrated in Fig. 16 are as follows: I—PV inverter is OFF and the microgrid frequency (f) is 50 ± 0.01 Hz. II—The PV inverter turns ON and the hybrid converter charges the battery with 20 $\mathrm{A_{dc}}$. III—The battery bank is still in bulk phase and more energy is harvested from the solar

Authorized licensed use limited to: N.C. State University Libraries - Acquisitions & Discovery S. Downloaded on June 16,2023 at 18:10:31 UTC from IEEE Xplore. Restrictions apply.

IPR2024-00389
Relink EX2003

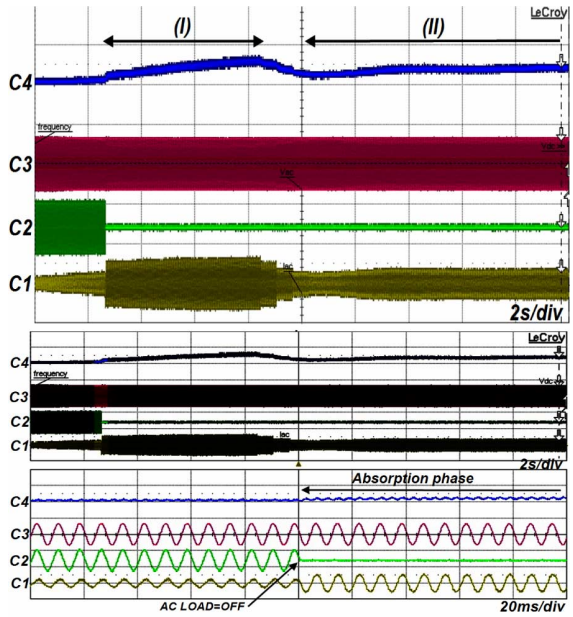

Fig. 17. Experimental results in off grid islanded mode: operation within anti-islanding limits. y-axis: C1—$I_{\rm ac}$ 10 A/div, C2—$I_{\rm acLOAD}$ 10 A/div, C3—$V_{\rm acPCC}$ 500 V/div, and C4—$V_{\rm dc}$ 5 V/div.

array. Notice on both intervals II and III, the frequency is disturbed but with negligible effect (maximum ± 0.1 Hz) by the PV inverter antiislanding algorithm. IV—The frequency limit is exceeded and the dc voltage steps down ($V_{\rm dc}$, 10 V/div) to the resting battery voltage and finally avoiding overcharging of the battery bank.

Fig. 17 illustrates the scenario, where both frequency generation and frequency-detection functions are implemented within the hybrid converter, respectively. PV inverter has the following phase transitions: I—AC load disconnects and the battery charge is in bulk phase and II—The battery voltage $V_{\rm dc}$ reaches the desired regulation set point and the PV inverter regulates its ac output current $I_{\rm ac}$ function of the frequency variation.

The hybrid converter can be programmed to perform a two-stage or three-stage charge profile by varying the microgrid line frequency in off-grid islanded mode. The PV inverter adjusts its output current based on the line frequency and ultimately regulating the dc voltage for the desired charging profile.

As an extended application, a load shedding mechanism can be implemented by using the PV energy primarily to charge the battery bank and the power management mechanism will give priority to the charge profile of the battery for multistage charging algorithm.

VI. Conclusion

The power converter system integration with renewable energy sources and interaction within a microgrid structure has been presented with applicability in off-grid islanded, grid-connected, and genset-connected mode for residential and commercial installations. The system architecture presented incorporates DPG modules with flexible modes of operation in order to control the power flow for energy prioritization and system-efficiency maximization. Different energy sources are integrated within the microgrid system, where the experimental results illustrate stable and robust DPG control operation under transient and dynamic conditions at the dc and ac port. The pseudodroop control structure is implemented at the DPG device level and without additional hardware or communication wiring interfaces between the hybrid converter and PV inverter devices. In off-grid islanded mode, when the energy provided by the PV inverter flows into the bidirectional hybrid converter, the dc battery voltage or current reaches unacceptable levels. The control method was proposed as implementation within the hybrid converter, where the FGF varies the line frequency with a specific frequency change rate related to the dc change rate. The PV inverter ceases to convert power until the line-frequency limits are restored to the normal range, as the dc level is within the specified set point limits. The agent of communication is the line frequency, which is precisely controlled by the hybrid converter. Furthermore, the PV inverter control is enhanced with the implementation of frequency-detection function, which continuously monitors the microgrid line frequency and reduces its power, if a specific pattern is detected while the hybrid converter varies the line frequency determined by the desired battery-charging profile.

References

[1] R. Erickson and D. Maksimovic, *Fundamentals of Power Electronics*, 2nd ed. New York: Springer, 2001, Ch. 18.
[2] C. Lascu, L. Asiminoaei, I. Boldea, and F. Blaabjerg, "Frequency response analysis of current controllers for selective harmonic compensation in active power filters," *IEEE Trans. Power Electron.*, vol. 56, no. 2, pp. 1826–1835, Feb. 2009.
[3] F. Blaabjerg, R. Teodorescu, M. Liserre, and A. Timbus, "Overview of control and grid synchronization for distributed power generation systems," *IEEE Trans. Ind. Electron.*, vol. 53, no. 5, pp. 1398–1409, Oct. 2006.
[4] M. Brenna, G. C. Lazaroiu, G. Superti-Furga, and E. Tironi, "Bidirectional front end converter for DG with disturbance insensitivity and islanding-detection capability," *IEEE Trans. Power Del.*, vol. 23, no. 2, pp. 907–914, Apr. 2008.
[5] T. Kerekes, R. Teodorescu, and U. Borup, "Transformerless photovoltaic inverters connected to the grid," in *Proc. 22nd Annu. IEEE Appl. Power Electron. Conf. 2007*, Feb./Mar., pp. 1733–1737.
[6] M. Dai, M. Marwali, J. Jung, and A. Keyhani, "Power flow control of a single distributed generation unit," *IEEE Trans. Power Electron.*, vol. 23, no. 1, pp. 343–352, Jan. 2008.
[7] E. Serban, M. Ngosi, and T. Monk, "Parallel operation of multi-mode Voltage Source Inverter modules with equal load sharing in single phase AC systems," in *Proc. IEEE OPTIM Conf.*, Brasov, Romania, May 2008, pp. 319–326.
[8] J. M. Guerrero, L. G. Arcia de Vicuna, J. Matas, M. Castilla, and J. Miret, "A wireless controller to enhance dynamic performance of parallel inverters in distributed generation systems," *IEEE Trans. Power Electron.*, vol. 19, no. 5, pp. 1205–1213, Sep. 2004.
[9] Y. A. Mohamed and E. F. El-Saadany, "Adaptive decentralized droop controller to preserve power sharing stability of paralleled inverters in distributed generation microgrids," *IEEE Trans. Power Electron.*, vol. 23, no. 6, pp. 2806–2816, Nov. 2008.
[10] T.-L. Lee and P.-T. Cheng, "Design of a new cooperative harmonic filtering strategy for distributed generation interface converters in an islanding network," *IEEE Trans. Power Electron.*, vol. 22, no. 5, pp. 1919–1927, Sep. 2007.
[11] F. Katiraei and M. R. Iravani, "Power management strategies for a microgrid with multiple distributed generation units," *IEEE Trans. Power Syst.*, vol. 21, no. 4, pp. 1821–1831, Nov. 2006.

Authorized licensed use limited to: N.C. State University Libraries - Acquisitions & Discovery S. Downloaded on June 16,2023 at 18:10:31 UTC from IEEE Xplore. Restrictions apply.

IPR2024-00389
Relink EX2003

[12] P. Rodriguez, A. Timbus, R. Teodorescu, M. Liserre, and F. Blaabjerg, "Reactive power control for improving wind turbine system behavior under grid faults," *IEEE Trans. Power Electron.*, vol. 24, no. 7, pp. 1798–1801, Jul. 2009.
[13] H. Karimi, A. Yazdani, and R. Iravani, "Negative-sequence current injection for fast islanding detection of a distributed resource unit," *IEEE Trans. Power Electron.*, vol. 23, no. 1, pp. 298–307, Jan. 2008.
[14] J. Stevens, R. Bonn, J. Ginn, S. Gonzales, and G. Kern, *Development and testing of an approach to anti-islanding in utility-interconnected photovoltaic systems*, SAND 2000-1939, 2000.
[15] D. Yazdani, A. Bakhshai, G. Joos, and M. Mojiri, "A nonlinear adaptive synchronization technique for grid-connected distributed energy sources," *IEEE Trans. Power Electron.*, vol. 23, no. 4, pp. 2181–2186, Jul. 2008.
[16] D. Sera, R. Teodorescu, J. Hantschel, and M. Knoll, "Optimized maximum power point tracker for fast-changing environmental conditions," *IEEE Trans. Ind. Electron.*, vol. 55, no. 7, pp. 2629–2637, Jul. 2008.
[17] J. M. Kwon, B. H. Kwon, and K. H. Nam, "Three-phase photovoltaic system with three-level boosting MPPT control," *IEEE Trans. Power Electron.*, vol. 23, no. 5, pp. 2319–2327, Sep. 2009.
[18] H. Kim, T. Yu, and S. Choi, "Indirect current control algorithm for utility interactive inverters in distributed generation systems," *IEEE Trans. Power Electron.*, vol. 23, no. 3, pp. 1342–1347, May 2008.
[19] S. Kuszmaul, S. Gonzalez, A. Ellis, and E. Serban, "Commanding inverters to establish coordinated μgrid functionality at Sandia National Laboratories," *Proc. IEEE 34th IEEE Photovoltaic Spec. Conf.*, pp. 1513–1518, Jun. 2009.
[20] D. Georgakis, S. Papathanassiou, N. Hatziargyriou, A. Engler, and C. Hardt, "Operation of a prototype Micro-grid system based on microsources equipped with fast-acting power electronics interfaces," in *Proc. IEEE 35th Ann. Power Electr. Spec. Conf. (PESC 2004)*, Jun., vol. 4, pp. 2521–2526.
[21] Y. W. Li and C. N. Kao, "An accurate power control strategy for power-electronic-interfaced distributed generation units operating in a low-voltage multibus microgrid," *IEEE Trans. Power. Electron.*, vol. 24, no. 12, pp. 2977–2988, Dec. 2009.
[22] J. M. Guerrero, L. Garcia de Vicuna, J. Matas, M. Castilla, and J. Miret, "Output impedance design of parallel-connected UPS inverters with wireless load-sharing control," *IEEE Trans. Ind. Electron.*, vol. 52, no. 4, pp. 1226–1135, Aug. 2005.
[23] J. M. Guerrero, N. Berbel, J. Matas, L. Garcia de Vicuna, and J. Miret, "Decentralized control for parallel operation of distributed generation inverters in microgrids using resistive output impedance," *IEEE Trans. Ind. Electron.*, vol. 54, no. 2, pp. 994–1004, Apr. 2007.
[24] J. M. Guerrero, L. Hang, and J. Uceda, "Control of distributed uninterruptible power supply systems," *IEEE Trans. Ind. Electron.*, vol. 55, no. 8, pp. 2845–2859, Aug. 2009.
[25] S. Mallat, *A Wavelet Tour of Signal Processing*. San Diego, CA: Academic, 1999, Ch. 4.
[26] M. Misiti, Y. Misiti, G. Oppenheim, and J. M. Poggi, *Wavelets and Their Application*. Washington, DC: ISTE, 2007, Ch. 4–6.
[27] M. Soma, W. Haileselassie, and J. Sherrid, "Measurement of phase and frequency variations in radio-frequency signals," in *Proc. IEEE 21st IEEE VLSI VTS 2003*, pp. 203–207.

Emanuel Serban (M'99–SM'09) received the B.Sc.E.E. and M.Sc.E.E. degrees from the University Politehnica of Timisoara, Timisoara, Romania, in 1994 and 1995, respectively.

In 1997, he joined Xantrex Technology Inc., where he was involved in the research and development on advanced switch-mode power electronics products. Since 2009, he has been with the Renewable Energies Business, Schneider Electric, Burnaby, BC, Canada, where he is currently a Senior Power Electronics Design/Research Engineer. His research interests include power electronics modeling and control, analysis and design of power converters for renewable and distributed energy systems.

Helmine Serban (M'08) received the B.Sc. and M.Sc. degrees in electrical engineering from the University Politehnica of Timisoara, Timisoara, Romania, in 1994 and 1995, respectively.

She is currently a Senior Lecturer at Simon Fraser University, Surrey, BC, Canada. Her research interests include digital signal processing and embedded systems.

Authorized licensed use limited to: N.C. State University Libraries - Acquisitions & Discovery S. Downloaded on June 16,2023 at 18:10:31 UTC from IEEE Xplore. Restrictions apply.

IPR2024-00389
Relink EX2003